JACS
JOURNAL OF THE AMERICAN CHEMICAL SOCIETY

Article

pubs.acs.org/JACS

Prodigious Effects of Concentration Intensification on Nanoparticle Synthesis: A High-Quality, Scalable Approach

Curtis B. Williamson,[†,§] Douglas R. Nevers,[†,§] Tobias Hanrath,[*,†] and Richard D. Robinson[*,‡]

[†]School of Chemical and Biomolecular Engineering and [‡]Department of Materials Science and Engineering, Cornell University, Ithaca, New York 14853, United States

Supporting Information

ABSTRACT: Realizing the promise of nanoparticle-based technologies demands more efficient, robust synthesis methods (i.e., process intensification) that consistently produce large quantities of high-quality nanoparticles (NPs). We explored NP synthesis via the heat-up method in a regime of previously unexplored high concentrations near the solubility limit of the precursors. We discovered that in this highly concentrated and viscous regime the NP synthesis parameters are less sensitive to experimental variability and thereby provide a robust, scalable, and size-focusing NP synthesis. Specifically, we synthesize high-quality metal sulfide NPs (<7% relative standard deviation for $Cu_{2-x}S$ and CdS), and demonstrate a 10−1000-fold increase in $Cu_{2-x}S$ NP production (>200 g) relative to the current field of large-scale (0.1−5 g yields) and laboratory-scale (<0.1 g) efforts. Compared to conventional synthesis methods (hot injection with dilute precursor concentration) characterized by rapid growth and low yield, our highly concentrated NP system supplies remarkably controlled growth rates and a 10-fold increase in NP volumetric production capacity (86 g/L). The controlled growth, high yield, and robust nature of highly concentrated solutions can facilitate large-scale nanomanufacturing of NPs by relaxing the synthesis requirements to achieve monodisperse products. Mechanistically, our investigation of the thermal and rheological properties and growth rates reveals that this high concentration regime has reduced mass diffusion (a 5-fold increase in solution viscosity), is stable to thermal perturbations (~64% increase in heat capacity), and is resistant to Ostwald ripening.

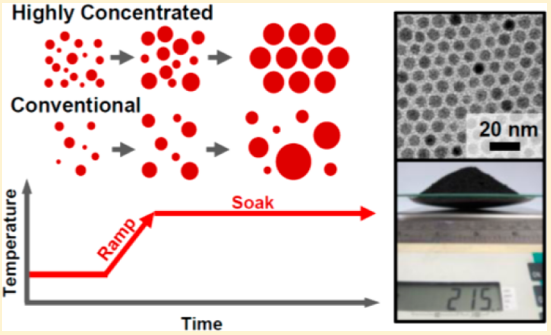

INTRODUCTION

By virtue of their size-tunable properties and facile solution processing, colloidal semiconductor nanoparticles (NPs), or quantum dots, have garnered intensive research interest as building blocks for many applications from optoelectronics to biological imaging.[11−14] The successful commercialization of promised NP technologies hinges critically on the development of scalable fabrication methods to provide technologically significant quantities of high-quality NPs (i.e., monodisperse size and composition). In the laboratory, monodisperse colloidal NPs are typically produced by a hot-injection method, in which organic-phase reagents are rapidly injected and mixed at high temperatures (>200 °C) and reacted for a short duration (<10 min).[15−17] This hot-injection method has played a key role in advancing NP science by providing access to a broad library of NP sizes, shapes, and compositions.[1,11,12,18] Unfortunately, high-quality NPs produced in the laboratory by hot injection result from small-scale reactions (roughly <100 mg yield[19]). A key barrier to scaling up hot-injection methods is the stringent demand for rapid precursor mixing required by the rapid reaction kinetics. For larger reactor volumes, mixing is slower, which introduces obvious impediments to reproducibility and control. Moreover, there is a need for efficient synthesis methods to enable economical fabrication at scale that produce high-quality NPs with high yields (>70%).

Attempts by the NP research community to resolve these scale-up challenges have led to several developments, including (1) novel precursors,[1,20] (2) seeded growth,[21] (3) heat-up methods,[20,22,23] (4) excess metal concentrations,[4,19] and (5) high solid loading.[4,9,19] For instance, recent work using novel precursors has enabled promising strides in high-quality NP synthesis and reaction control (e.g., ammonium sulfide[20] and thioureas[1]). Alternatively, using a hot-injection method, Cademartiri et al. demonstrated that a high Pb precursor loading (423 g/L) can be used to synthesize 1.5 g, including ligands, of monodisperse PbS NPs (~8% size dispersion based on photoluminescence (PL), in a 50 mL reaction).[4] Although this work revealed the merit of using a high precursor loading to achieve monodisperse NPs, further scale-up of this method is hindered by the need for a rapid injection and unknown kinetics of the heterogeneous reaction. Furthermore, a substantial portion of the precursor remains unreacted (and is discarded), reducing the production yield (mass of NP product per reaction volume) and synthesis efficiency. Figure 1 provides a summary of the efforts made by the NP community to scale-up NP syntheses, and a comparison to our experimental production yields reported here.

Received: September 23, 2015
Published: November 22, 2015

DOI: 10.1021/jacs.5b10006
J. Am. Chem. Soc. 2015, 137, 15843−15851

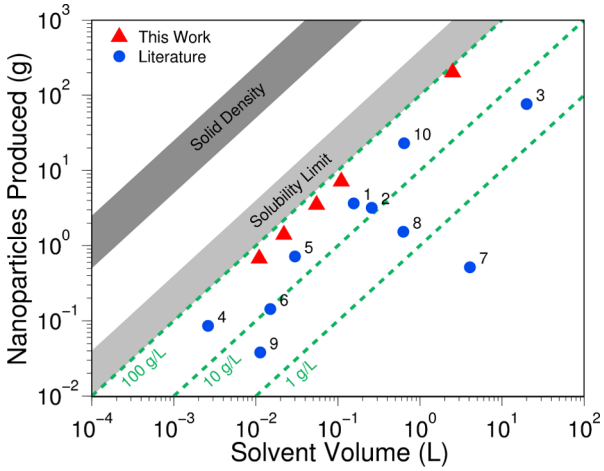

Figure 1. Scaling efforts: comparison of experiments from this work to literature reports based on the theoretical maximum possible NP yield. Production yields are depicted by the green hash lines, and are a ratio of the full conversion of the limiting reagent to the total reaction volume. Approximate precursor solubilities in long-chain organic solvents and solid precursor densities are displayed in the light and dark gray regions, respectively. Literature materials: (1) PbS,[1] (2) Fe_2O_3,[2] (3) CdSe,[3] (4) PbS,[4] (5) PbS,[5] (6) CuS,[6] (7) $CISe_2$,[7] (8) CdSe,[8] (9) CdSe,[9] and (10) PbS.[10]

Compared to the conventional hot-injection method, the gradual heat-up synthesis offers more design flexibility and quality control, specifically for NP synthesis at large scales. The heat-up approach has already been demonstrated in the synthesis of metal oxide[16,22] and metal sulfide[10,20,24,25] NPs. Notably, some heat-up method use a "one-pot" approach, where all reagents are mixed together initially; unfortunately, this convolutes the precursor dissolution and reaction rates, and hinders consistent production of high-quality NPs.[23] Decoupling the dissolution and reaction rates is a key "current challenge" for heat-up methods.[23] Vis-à-vis scale-up, an important advantage of the heat-up method is that precursor mixing and growth reaction are temporally decoupled; this is achieved by thoroughly mixing the precursors at low temperatures (to reduce the reaction rates and enable a prolonged mixing phase), and then heating the mixed solution to initiate NP growth. To further advance the heat-up method toward large-scale synthesis, several key challenges must be resolved, namely, to (1) ensure burst nucleation during the heat-up stage, (2) control the growth rates to enable size-focusing, and (3) maintain temperature uniformity through the ramp and growth stages.[23] Lastly, fine control over NP growth rates and system stability to perturbations are essential for successful scale-up.

We embraced these challenges as an opportunity to investigate a previously unexplored regime of nanoparticle synthesis: precursor concentrations near the solubility limit. We seek to answer the central question of how the nanosynthetic chemistry of the heat-up method differs when the concentrations are intensified. We find that this new regime provides a unique approach to enable a size-focusing, self-stabilizing NP synthesis. Specifically, we demonstrate that highly concentrated reagent solutions produce (a) slow and size-focusing growth, (b) monodisperse NPs (<7%), (c) delayed Ostwald ripening, and (d) high yield. We verified the robust scalability of our process by rigorous reproducibility and spike sensitivity tests. In comparison to conventional NP synthesis (<8 g of NPs/L of solvent[1,2,26]), our highly concentrated heat-up method provides a 10-fold improvement in NP volumetric production capacity: 86 g of NPs/L of solvent. High concentration and high precursor conversion enable process intensification: supplying efficient use of reagents, solvent, and reactor volume to produce high-quality NPs. We focus on copper(I) sulfide ($Cu_{2-x}S$) as a model system to more complex ternary copper sulfides (e.g., copper indium sulfide), which are a promising nontoxic alternative to cadmium and lead salt semiconductor NPs.[27] We also demonstrate how the highly concentrated heat-up method can be successfully generalized to PbS and CdS NPs. Through property characterization and modeling, we find that this highly concentrated regime creates fortuitous synthesis conditions by providing an increase in thermal stability that absorbs temperature perturbation and a decrease in mass diffusivity that protects the system from Ostwald ripening.

RESULTS

Concentration Effects. To enable robust and reliable synthesis of monodisperse NPs, three conditions must be met: (1) nucleation burst, (2) size-focusing growth, and (3) delayed Ostwald ripening.[16,28] In this work we show that these conditions can be met by using a heat-up method,[20,22] and substantially increasing precursor concentrations beyond conventional NP synthesis conditions (see Table S1 for experimental details). In the discussion below, we will refer to concentrations employed in traditional NP synthesis (~100 mM) as "conventional" in contrast to the "highly concentrated" conditions (i.e., 1000 mM) near the maximum solubility or saturation limit for the precursor in the reaction solvent. On the basis of a literature survey of conventional syntheses, typical precursor concentrations are 1−2 orders of magnitude lower, ranging from 10 to 100 mM (see Table S2 for a detailed comparison).

The basic aspects of our heat-up synthesis are schematically illustrated in Figure 2. Organic-phase precursors are first mixed at 50 °C to ensure a uniform solution concentration and the suppression of particle growth; then the solution is heated to and maintained (i.e., soaked) at 185 °C to grow the NPs. At the low-temperature mixing stage, both the conventional and highly concentrated reactions consist of small polydisperse NP seeds (~3 nm). However, as these seeds are heated to 185 °C, the conventional and highly concentrated conditions produce greatly divergent results: under conventional conditions the seed NPs grow into a polydisperse set, but at highly concentrated conditions the particles size-focus and become monodisperse (Figure 2).

The evolution of the NP size and relative standard deviation (RSD) during the extended soak at 185 °C differs significantly for conventional and highly concentrated conditions (Figure 3). The RSD is defined as the ratio of the standard deviation over the mean NP diameter. To quantify the evolution of the NP diameter and RSD, we extract aliquots and measure the size distribution for a large particle set (statistical NP size analysis is provided in the Supporting Information, Figures S1 and S2 and Table S1). Low concentrations (<500 mM) yield rapid particle growth (~2.5 nm/h) with extensive broadening of the size distribution (15−20% RSD). In contrast, more concentrated solutions (≥500 mM) result in significantly slower particle growth (~0.25 nm/h) and a narrowing size distribution (7−12% RSD). Specifically, as the soak time increases, the conventional concentration produces NPs that continue to increase in size (5.7 nm at 0 h to 14.7 nm at 4 h, Figure 3b), while the high concentrations (≥500 mM) produce NPs that

DOI: 10.1021/jacs.5b10006
J. Am. Chem. Soc. 2015, 137, 15843−15851

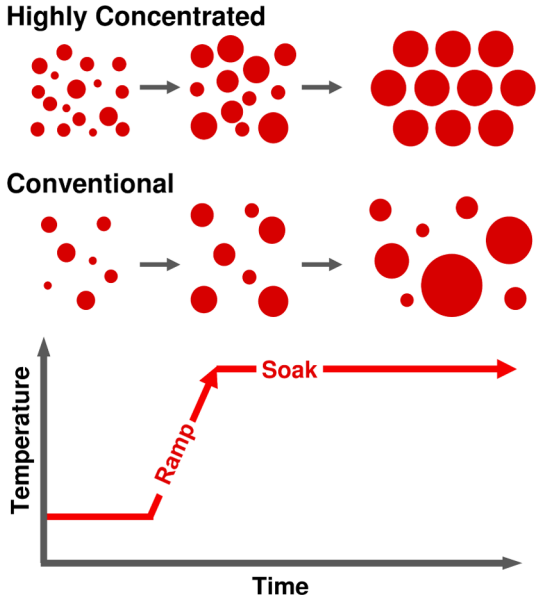

Figure 2. Reaction mechanism: comparison of the new highly concentrated approach to the conventional NP reaction concentration using a heat-up method. Initially, both NP concentrations are the same in size and dispersion. Divergence between concentrations occurs upon soaking the NPs for an extended duration. The highly concentrated solution size focuses and becomes monodisperse, whereas the conventional synthesis experiences Ostwald ripening.

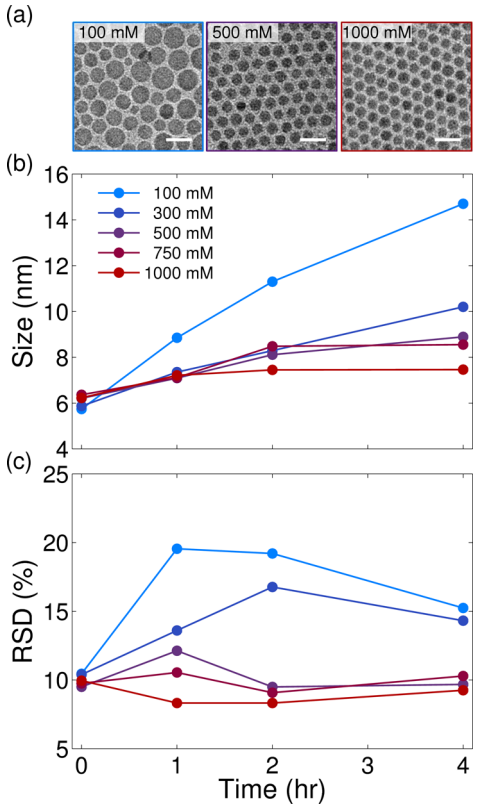

Figure 3. Effect of the precursor concentration on NP size and quality: (a) TEM images, (b) size, and (c) relative standard deviation (RSD) of $Cu_{2-x}S$ NPs at various CuCl concentrations over a 4 h soak at 185 °C. For concentrations below 500 mM, NPs experience Ostwald ripening with time. At concentrations of 500 mM and higher, NP solutions are at equilibrium with approximately constant size and RSD with time. TEM images in (a) are color correlated to the 100, 500, and 1000 mM reactions to illustrate the size and quality of the NPs. Scale bars represent 20 nm.

grow slowly (e.g., 500 mM NPs are 6.2 nm at 0 h and 8.9 nm at 4 h, Figure 3b).

More striking is the effect of the concentration on the RSD: at the conventional concentration (100 mM), the RSD increases from 10% at 0 h to 18% at 2 h (Figure 3c), but for concentrations ≥500 mM, the RSD decreases; particularly for the highly concentrated solution (1000 mM), the RSD remains constant with time: 9.6% at 0 h and 9.8% at 2 h (Figure 3c). The "apparent" size-focusing (decrease in RSD) for lower concentrations (<500 mM) at longer times is an artifact of the NP size increasing faster than the absolute standard deviation, resulting in a decreasing RSD (see Figure S2 for absolute standard deviation vs time). The experimental data clearly illustrate that higher precursor concentrations produce small, monodisperse particles that focus in size over extended reaction growth or soak times. The results further suggest that the crossover point for the size-focusing behavior occurs near ≥500 mM. Notably, the RSD achieved in this synthesis is significantly smaller than in previously reported $Cu_{2-x}S$ NPs (typically >14% RSD).[1,25,29−32] The consistent narrow size distribution of NPs at extended soak times at 185 °C suggests that the colloidal stability of NPs fabricated by the heat-up method is greater than that of NPs fabricated by hot injection.

To explain the experimental trends observed in the heat-up synthesis, we hypothesize that the nucleation and growth steps are temporally decoupled. To test this hypothesis, we extended the duration of the low-temperature (50 °C) mixing stage for 4 h after mixing the precursors together (Figure S3). Both the conventional and highly concentrated reactions maintained a constant size (~3 nm) and RSD (20% RSD) during the 4 h, indicating a stable nucleation stage at 50 °C, and the successful separation of nucleation and growth via the heat-up method. Furthermore, we probe the effects of slow precursor mixing (occurring over the course of 3 min instead of instantly) and still obtain high-quality products, illustrating that our method is not dependent on a rapid injection of precursors (see Figure S4).

Beyond the $Cu_{2-x}S$ system, we demonstrate the general applicability of the highly concentrated heat-up method to other materials, namely, PbS and CdS. Similar to the $Cu_{2-x}S$ system, 1000 mM concentrations of lead oleate and cadmium oleate are mixed with a sulfur source (5000 mM sulfur oleylamine for PbS or 2500 mM trioctylphosphine sulfide for CdS). Ramp−soak heating profiles identical to those of the $Cu_{2-x}S$ system are used (ramp up to and maintain at 185 °C). For the PbS NP system, the NP size and RSD of 7.0 nm and 17.5%, respectively, experience slow growth and size-focusing throughout the 4 h soak (the size and RSD at 2 h are 7.8 nm and 15.1%, respectively; see Figure S5). Similarly, CdS NP synthesis at high concentrations has restricted growth during the long reaction duration. After 15 min into the soak, the absorbance edge does not shift, demonstrating that particle growth has ceased (see Figure S6). Furthermore, the full width at half-maximum (fwhm) of the PL peak for the CdS NP remains constant during the soak (the fwhm of the PL peak is 25 nm). The optically determined size and RSD are 4.8 nm and 7%, respectively. This is in close agreement with the measured size and RSD from the TEM image at 0 h into the soak. The stabilized particle growth of PbS and CdS NPs, as well as the

DOI: 10.1021/jacs.5b10006
J. Am. Chem. Soc. 2015, 137, 15843−15851

constant RSD, in the highly concentrated heat-up approach exhibits substantial synthesis control, which is essential to the scale-up of these materials.

Reproducibility. To characterize batch-to-batch reproducibility, we performed triplicate control experiments for the 100 mM (conventional) and 1000 mM (highly concentrated) systems under otherwise identical synthesis conditions. The average of three replicate reactions is portrayed in Figure S7, with error bars representing the standard deviation of the size and RSD between the reactions. Replicated reactions for the conventional concentrations produce NP mean size and RSD that have considerable variations between reactions (up to ~15% variability in size and 5% variability in RSD). However, the highly concentrated reactions result in consistent sizes and RSDs (<5% variability).

Reaction Equilibrium Sensitivity. To characterize the sensitivity of the reaction equilibrium exhibited by the highly concentrated system, we perturbed the system with various chemical spikes, a 10 vol % spike of three different 1000 mM chemical solutions: (1) dissolved copper chloride precursor, (2) dissolved elemental sulfur precursor, and (3) ~3.0 ± 1.0 nm $Cu_{2-x}S$ seeds (NPs from the 50 °C mixing stage of a 1000 mM reaction solution). These experiments consisted of a 1000 mM medium (copper and sulfur precursors) initially mixed at 50 °C that was heated to and maintained at 185 °C for 2 h, after which the reaction solution was spiked with one of the three spike solutions. Aliquots of each spike test were taken before the spike at 0 min (0 min is defined as the beginning of the soak phase, when the solution has just reached 185 °C), 60 min, 120 min, and after the spike at 125 min (5 min postspike), 150 min (30 min postspike), 180 min, and 240 min. The size and RSD of the NPs for the various spike tests are shown in Figure 4. The inset in Figure 4 shows the responses to the three spikes. Notably, the highly concentrated solution is quickly restored to equilibrium after chemical perturbation, via seeds or the copper precursor, and is thus less susceptible to batch-to-batch chemical variations and local concentration variations within a solution.

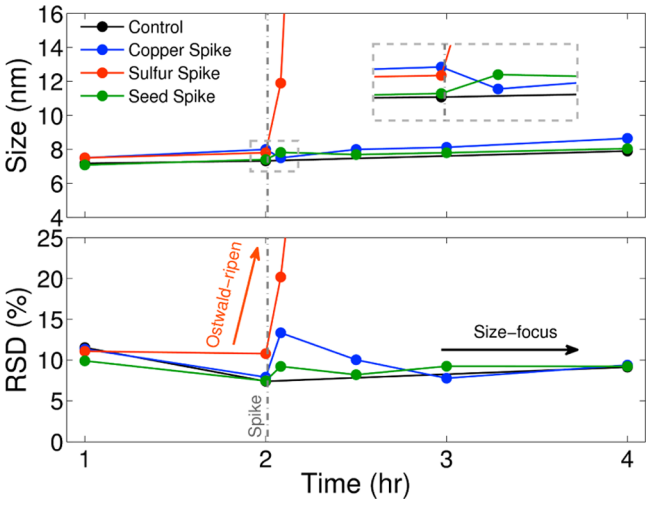

Figure 4. Reaction robustness: concentrated reactions spiked with three different starting chemicals, 1000 mM CuCl, 1000 mM S, and 1000 mM equivalent $Cu_{2-x}S$ seeds in an oleylamine (OLA)/1-octadecene (ODE) mixture. The spike is injected after the 2 h aliquot. The inset zooms in on the behavior of the spike: (1) copper decreases the average size, (2) sulfur induces Ostwald ripening, and (3) the seeds increase the average size. Spiking with copper and seeds leads to size-focusing within 1 h.

Upon spiking the system with the copper chloride solution, a sudden decrease in the average particle size occurs with a corresponding increase in the RSD. The quality of the NPs at 5 min postspike is similar to that observed at the top of the ramp (time 0 h). One hour after the spike, the NP distribution recovers to the original prespike size and RSD values. We associate this change in size and RSD with the spontaneous shift in chemical equilibrium, resulting from the etching of loosely bonded sulfur to form new seeds.

In sharp contrast to the copper chloride spike, the sulfur spike destabilizes the NP growth. We found that a sulfur spike results in a massive increase in size and RSD (Figure 4), both of which escalate as the soak progresses. Five minutes after the spike, the particle size and RSD double, and continue to ~1000 nm and ~1000% by 4 h. The sulfur spike can be viewed as a large source of anions that dampen repulsions between positively charged particles, increasing NP collisions and growth rates.[33] To understand the charge on the NPs, we measured the surface potentials of purified NPs (prior to spike) via dynamic light scattering (DLS), and the maximum surface ζ potential of our particles is approximately +50 mV (Figure S8). A ζ potential of +50 mV is indicative of highly stabilized positively charged particles.[34,35] The large NPs resulting from the sulfur spike aggregate and precipitate out of solution, preventing a more in-depth DLS analysis. Fast particle precipitation suggests the surface potential is near 0 mV. Enhanced collisions (coalescence) reasonably explain the significant particle growth. Furthermore, we relate the increase in sulfur concentration caused by the sulfur spike to a decrease in the overall solution stoichiometry (Cu:S ratio) or sulfur-rich conditions (see Figure S9). Reactions rich in sulfur yield extremely large (>100 nm) NPs, similar to the sulfur spike.

As a third robustness test, we also spiked the system with $Cu_{2-x}S$ seed particles (3 nm, 20% RSD) from the mixing phase at 50 °C. Upon injection of these seeds into the NP soaking solution, there is an abrupt increase in both size and RSD at 5 min after the spike. This response is not a bimodal distribution of sizes, but rather a single distribution at a slightly larger particle size (see the inset of Figure 4). The rapid disappearance of the seeds after the spike implies that the injected particles had combined either with the native NPs or with each other to form larger NPs.

Synthesis Scale-Up. The long-time stability of NPs in highly concentrated solutions and the robust system recovery from small chemical perturbations are desirable attributes for scale-up, which makes this synthesis method ideal for large-scale reactions. To test this assertion, we demonstrate the transition from a traditional laboratory-scale NP synthesis to a large-scale pilot reaction. We scaled a typical laboratory batch reaction volume (~25 mL) by 2 orders of magnitude to 2.5 L using a 4 L reactor and an overhead stirrer with a crescent paddle blade (Figure 5). Following the protocol developed for small-scale reactions with the optimal highly concentrated conditions of 1000 mM CuCl and 5000 mM S, the sulfur precursor is injected into the reaction vessel containing the copper precursor at 50 °C and mixed. Similar to the small-volume reactions, a 6 °C temperature spike is observed postinjection, suggesting similar precursor conversion. We heat the solution to 185 °C and hold at this temperature for 2 h. The reaction cools via a water bath to 100 °C, at which point 2

DOI: 10.1021/jacs.5b10006
J. Am. Chem. Soc. 2015, 137, 15843−15851

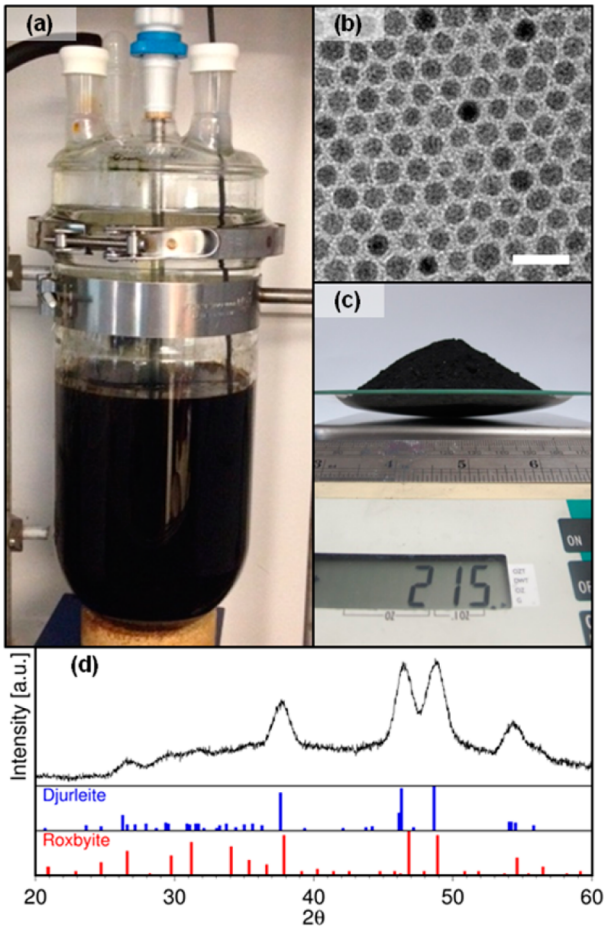

Figure 5. Large-scale reaction: (a) 2.5 L reaction of $Cu_{2-x}S$ nanoparticles. The solution is mixed via an overhead stirrer at 700 rpm. (b) TEM images of $Cu_{2-x}S$ nanoparticles with an average size and RSD of 8.0 nm and 9.3%, respectively. TEM images are consistent with various samplings of the final product. The white scale bar on the TEM image represents 20 nm. (c) Total recovered product of 215 g from the reaction vessel after purification and drying. (d) XRD pattern of collected NP powder. The pattern is a mix between the djurleite ($Cu_{1.94}S$, PDF no. 00-023-0959) and roxbyite ($Cu_{1.8}S$, PDF no. 00-023-0958) phases.

L of ethanol quenches the solution to room temperature. The precipitated product is further purified through centrifugation.

We successfully recovered 215 g of purified product. To verify batch consistency, we measured samples from six different centrifuge tubes at various purification times (TEM images provided in Figure S10). The sample to sample variability in the product (size and RSD) is less than 5%. The average NP size is 8.0 nm with an RSD of 9.3%. X-ray diffraction (XRD) shows the particles are a mix between the djurleite ($Cu_{1.94}S$) and roxbyite ($Cu_{1.8}S$) phases (see Figure 5 and Figures S11 and S12). Thermogravimetric analysis (TGA) reveals considerable mass loss at 300 °C, near the normal boiling point of oleylamine (see Figure S13). We associate this TGA signature with the loss of oleylamine ligand, which contributes approximately 20 wt % of the total collected mass. Factoring this into the theoretical conversion, we obtained a total Cu_2S conversion of greater than 93%.

DISCUSSION

To understand the possible mechanisms that lead to this unexpected stability and size control at high concentrations, we examine three factors that provide insight into the process at high concentrations, namely, (1) the solution viscosity increases by a factor of 5, reducing mass diffusion, (2) the heat capacity increases by ∼64%, and (3) the influence of Ostwald ripening on NP growth decreases. We will discuss each of these parameters in detail below.

Viscosity Effects. An important consequence of concentrating the precursor is a significant increase in viscosity of both the unreacted precursor and the reacted NP solutions. To better quantify the rheological properties of the reaction solution, we performed parallel plate rheology measurements on the NP solutions at various concentrations (see the Supporting Information for details). Baseline measurements of the reaction mixture are made in reference to their organic matrix: 70% oleylamine/30% 1-octadecene. When the inorganic precursors ($Cu^{I}Cl$ and elemental sulfur) are mixed at 50 °C, both the conventional and highly concentrated solutions have similar viscosities that are greater than that of the baseline of the organic matrix (see Figure S14). However, at elevated temperature (120 °C), the viscosity of the conventional concentration solution (0.81 mPa·s) is similar to that of the organic matrix (0.77 mPa·s), whereas the highly concentrated solution viscosity (3.8 mPa·s) is nearly an order of magnitude greater than that of the organic matrix (see Figure 6a).

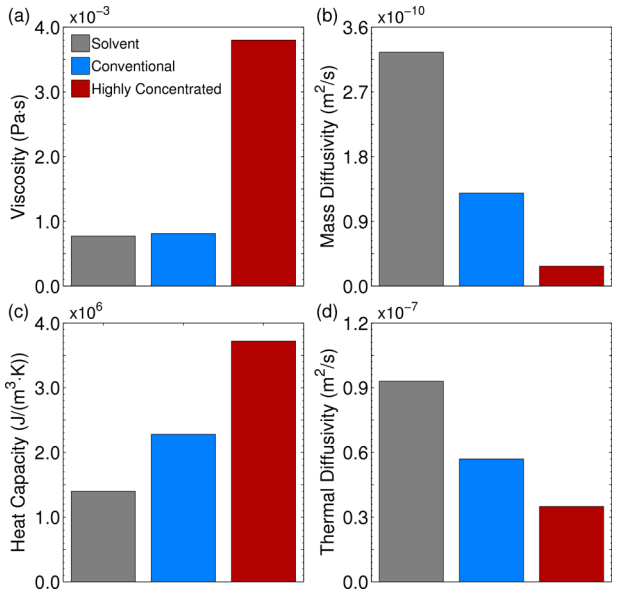

Figure 6. Experimental physical properties for conventional vs highly concentrated NP solutions: (a) viscosity and (c) heat capacity are directly correlated to the precursor concentration, while (b) mass and (d) thermal diffusivities are inversely correlated to the precursor concentration (see the Supporting Information, including Table S3, for the methods and details).

Interestingly, a concentration of , 500 mM corresponds to the critical turning point for both enhanced viscosity and size-focusing growth (see Figure 3 and Figure S14). The measured increase in solution viscosity with salts has been previously observed for NP-containing systems, namely, polymer NPs and oxide NP suspensions.[36,37] Dissociating salts present in colloidal solutions induce various electrostatic forces on the

DOI: 10.1021/jacs.5b10006
J. Am. Chem. Soc. 2015, 137, 15843−15851

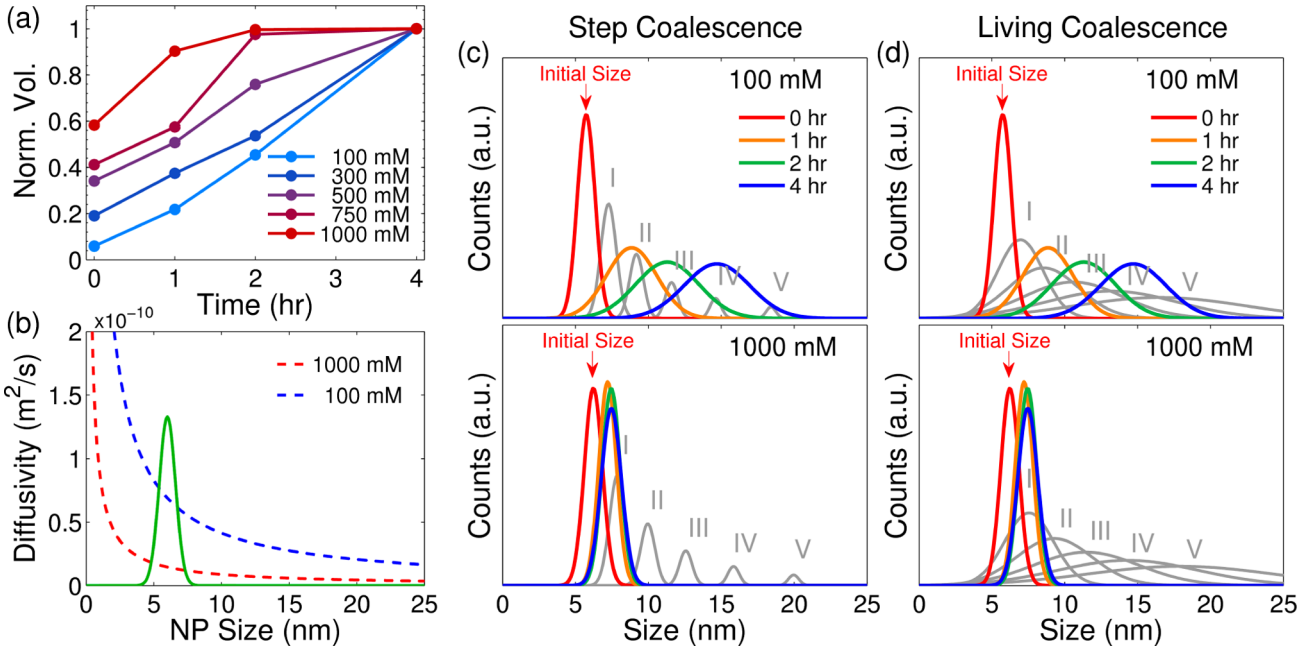

Figure 7. (a) Volumetric growth rate. The NP sizes for each concentration are converted to volume and normalized by the 4 h "final" volume. Linearly increasing volume with time indicates Ostwald ripening, where a sigmoidal dependence suggests coalescence or monomer addition. (b) Change in Stokes−Einstein diffusivity over various particle sizes at a constant solution viscosity for the 100 and 1000 mM reactions. The average initial size distribution for both concentrations is overlaid in green. The diffusivity in the 100 mM reaction is 5 times greater than the diffusivity in the 1000 mM reaction for the same size of NPs. (c, d) (Color curves) Mapping of the temporal evolution (0−4 h) of experimentally determined values, expressed as Gaussians of the mean size and SD of the conventional (top) and highly concentrated (bottom) reactions. (Gray curves) I−V correspond to a projection of the system after coalescence events, with each curve progression marking a halving of the number of particles from the previous curve (e.g., condition II has half the number of particles of condition I, and III half that of II). (c) Step coalescence represents an aggregation mechanism where each particle must coalesce once before any particle can coalesce twice, while (d) living coalescence represents a mechanism where some particles experience multiple coalescence events while others experience none.

suspended NPs that inhibit the molecular transport of fluid around these particles and thus increase the solution viscosity. Unlike these NP-containing solutions with salts, our solution is organic and reactive, in which the salts are our precursors. We hypothesize that the increased viscosity for highly concentrated solutions is induced by electrostatics and metal−π interactions (equivalent to H-bonding in aqueous systems) generated by the high chloride concentration and lone pair electrons (amines) within the solution.

In the context of NP motion through the reaction fluid, the viscosity (μ) can be translated to mass diffusivity (D) using the Stokes−Einstein−Sutherland equation (i.e., $D = k_B T/6\pi\mu r$) for NPs with hydrodynamic radius r. Comparing mass transport for concentrated and conventional conditions therefore shows that diffusivity in the highly concentrated condition is approximately 5-fold lower, given the differences in viscosity discussed above (Figure 6b and Table S3). We conclude that the reduced NP mobility in the concentrated reaction environment contributes significantly to the stability of the size distribution due to decreased NP collision rates (see the section "Growth Mechanism" below).

Heat Transport. Thermal conductivity and heat capacity can have a significant impact on NP reactions, especially since both factors depend on the NP concentration.[38−40] However, the impact of the thermal properties of the reaction fluid has not received the appropriate consideration in previous studies. We hypothesize that the higher heat capacity of the highly concentrated system renders it more robust relative to experimental thermal fluctuations. To test this hypothesis, we deliberately perturbed the reaction environment (maintained at 185 °C) with a spike of solvent at room temperature. As detailed in the Supporting Information (Figure S15), thermal fluctuations due to the spike are less pronounced in the concentrated system compared to those for the conventional conditions. The immediate temperature drop in the highly concentrated reaction is roughly half that of the conventional reaction, indicating that the former has a higher heat capacity and thus a smaller thermal diffusivity. This behavior agrees with the higher heat capacity (~64% greater) and lower thermal diffusivity measured for the highly concentrated solution (Figure 6c,d, Table S3).

Growth Mechanism. To better understand the growth mechanism, we can examine the precursor conversion rate and growth models on coalescence (or agglomeration) and Ostwald ripening. The precursor conversion is assessed through the dried NP mass, while excluding the mass of organic ligands as determined by TGA (see the Supporting Information for details, Figure S16). At the beginning of the soak stage at 185 °C (time 0 h), the conversions are nearly complete for both the conventional and highly concentrated conditions (82% and 88%, respectively); furthermore, both conditions have similarly sized NPs (~6 nm). The high conversion values indicate the concentration of the remaining active growth species (or residual precursor) is small. Specifically, if all of the residual precursor is considered to be in the form of Cu_2S monomer, the approximate residual concentration would be 8 and 50 mM Cu_2S for the conventional and highly concentrated solutions, respectively. In relation to the LaMer model, the fact that the conventional conditions undergo Ostwald ripening (to be discussed; see Figure 7) suggests that this solution is near the

DOI: 10.1021/jacs.5b10006
J. Am. Chem. Soc. 2015, 137, 15843−15851

monomer saturation limit (at approximately 8 mM Cu_2S monomer, Table S4) and that the residual monomer is in equilibrium with the monomer attached to the NP surface.[16,41] Thus, the highly concentrated solution, with a higher residual monomer concentration (approximately 50 mM), is still supersaturated, and resistant to Ostwald ripening.[4,41]

To describe the NP size evolution during the soak stage, we calculate the increase in NP size if all of the residual precursor were to be added as new material to the existing NPs (i.e., 100% conversion). The mean NP size increases by only ∼7% for the conventional case (from ∼6 to 6.4 nm), and ∼4% for the highly concentrated case (from ∼6 to 6.3 nm) (see the Supporting Information). However, experiments show that the final size for the conventional and highly concentrated cases (14.7 and 7.5 nm, respectively) is much greater than the size predicted by this simple calculation; this comparison indicates that another mechanism beyond monomer addition via unreacted precursor is required to describe the observed NP growth.

In light of the depleted monomer condition, we infer that the growth mechanism should be Ostwald ripening or NP coalescence, which would be governed by NP mobility or diffusivity rather than concentration gradients. Ostwald ripening is NP growth via NP dissolution to monomers, and then monomer deposition onto larger NPs.[16,41] One method to assess the growth process is to plot the time evolution of volume normalized by the final volume.[42,43] For the conventional concentrations, although the growth in particle size slows as the reaction progresses, the volumetric growth rate remains fairly constant over the duration of the experiment (Figure 7a, blue points, 100 mM). A linear volumetric growth rate is indicative of Ostwald ripening, as supported by the Lifshitz−Slyozov−Wagner (LSW) theory.[41,43−45] Alternatively, a sigmoidal curve describes the highly concentrated condition (Figure 7a, red points, 1000 mM), suggesting the growth process is through coalescence or monomer addition.[42,43]

Additionally, LSW theory correlates the volumetric growth rate of NPs to their diffusivity, in which greater particle diffusivity induces faster growth. We determined the diffusivity of our NPs via the Stokes−Einstein−Sutherland relation (vide supra)[33] (see the Supporting Information). Figure 7b shows the diffusivity of the conventional and highly concentrated reactions at various sizes with a constant viscosity. A Gaussian distribution of the experimentally determined particle size and deviation is overlaid (Figure 7b, green curve) on these diffusivities and represents the size and standard deviation (SD) of both concentrations at the beginning of the soak. Interestingly, the conventional reaction has a 5-fold greater diffusivity compared to the highly concentrated reaction, at the beginning of the soak. Furthermore, the variation in particle diffusivity for an identical NP size distribution is 5-fold larger in the conventional reaction. For instance, a 3σ (3-SD) particle spread (99.7% of total particles) corresponds to a variation or disparity in diffusivity of 4.55×10^{-11} m^2 s^{-1} for the conventional reaction, whereas the highly concentrated reaction only varies in diffusivity by 9.70×10^{-12} m^2 s^{-1} for the same NP size distribution. The higher diffusivities coupled with a larger variation in diffusivity over the particle distribution provide mechanistic insight into not only the faster particle growth of the conventional reaction, but also its observed increase in RSD (Figures 3 and 7a). Moreover, as the soak time increases and the NPs in the conventional condition grow in size, their diffusivity and variation in diffusivity decrease, resulting in slower growth and a constant but large SD (Figures 3 and 7b).

We investigated various growth models to describe the growth process for each concentration. Each model represents the data to a moderate degree of accuracy (see Table S5 for R^2 values). A model proposed by Huang et al.[46] suggests a two-term, three-fitting-parameter model, in which the first fitting parameter (k_1) describes orientated attachment (OA) and captures the initial sigmoidal growth behavior and the second fitting parameter (k_2) describes Ostwald ripening (OR) (Figure S17). The third parameter (n) is an arbitrary constant that scales the time dependence on Ostwald ripening. The fits for this model generally follow the suspected trends from our data: k_2 (OR) dominates at lower concentrations, whereas k_1 (OA) dominates in the highly concentrated case. Additionally, the calculated R^2 values are near unity for each concentration, which suggests the fits are accurate. However, the trends begin to deviate from the experimental data at the longer soak times (see Figure S17).

Kinetic growth profiles of NPs can also be described by the Kolmogorov−Johnson−Mehl−Avrami (KJMA) model (Figure S18),[47−51] which requires the normalization of the NP volumes, such that the bounds of the expression are between 0 and 1. Unlike the Huang model, this is a two-fitting-parameter model that does not describe Ostwald ripening, but rather only aggregative NP growth (k_g) or coalescence rate.[47,48] This rate increases with the concentration, suggesting coalescence is the dominant process at high concentrations, which agrees with the oriented attachment rate of the Huang model (see Figure S18). Lastly, we analyze our NP growth in context of the four-step NP agglomeration described by Finney et al.[42] Briefly, this model describes the evolution of the particle size in the context of rates for bimolecular agglomeration (k_3) and autocatalytic agglomeration (k_4).[42] This agglomeration (or coalescence) model provides a good fit to the experimentally observed particle size evolution shown in Figure 3 (see Figure S19). Notably, this analysis shows $k_4 > k_3$ at conventional concentrations, and a transition to $k_4 < k_3$ at high concentrations (see Figure S19). This model indicates that conventional concentrations are dominated by autocatalytic agglomeration or Ostwald ripening, whereas, at high concentrations, the NP synthesis is dominated by bimolecular agglomeration or coalescence. Importantly, the reduced overall agglomeration can be explained by two key experimental trends discussed above, namely, (1) a higher residual precursor concentration stabilizes the NP surface and thereby reduces the energetic driving force for agglomeration and (2) the rate of NP collisions per particle is reduced if the high viscosity of the synthesis environment increases. Ultimately, these growth models each suggest the same conclusion: conventional conditions grow via Ostwald ripening, and as the concentration increases, Ostwald ripening is suppressed. Furthermore, the models indicate the growth mechanism for high concentration is via coalescence.

To determine the magnitude of growth by coalescence, we compare the theoretical evolution in size distribution for NPs undergoing coalescence to our experimentally measured size distributions. Specifically, as an analogy to polymerization chemistry, two theoretical types of coalescence processes are considered: step coalescence and living coalescence (see the Supporting Information for model details). Step coalescence means that each particle must coalesce once before any particle can coalesce twice (or again). This would allow the NPs in

DOI: 10.1021/jacs.5b10006
J. Am. Chem. Soc. 2015, 137, 15843−15851

solution to follow similar growth trajectories and enables the NPs to equilibrate before the next coalescence step, thereby reducing the RSD (Figure 7c, gray curves). On the other hand, living coalescence means some particles may experience multiple coalescence events while others experience none. Hence, each particle experiences different growth trajectories, which consequently increase the RSD (Figure 7d, gray curves). Conceptually, living coalescence dominates when the probability of NP collisions is high, favoring multiple coalescence events involving the same particle. In contrast, step coalescence dominates when the probability that a particle experiences multiple coalescence events for a given time is low. Figure 7c,d illustrates the theoretical evolution of both step and living coalescence processes compared to our experimental data. Each shift in theoretical size distribution (e.g., I → II → III, gray curves) represents the system after the number of particles has been cut in half (e.g., condition II has half the number of particles of condition I, and III half that of II; see the Supporting Information for details). For step coalescence, this means each particle experiences one coalescence event between I and II, while, for living coalescence, each particle may experience a range of coalescence events. Thus, each NP involved in step coalescence follows a consistent reaction profile or experiences the same number of coalescence events, which promotes a uniform size distribution. The opposite is true for living coalescence. Comparing our data to these theoretical distributions suggests that conventional conditions are better described by living coalescence, whereas high concentrations are better described by step coalescence, notably with only one step (see Figure 7c,d).

Physically, the larger NP mass diffusivities for the conventional reactions enable some NPs to experience multiple coalescence events while other NPs in the system experience few or none, promoting a range of NP growth trajectories and increasing RSD. In contrast, NPs in high concentration reactions diffuse more slowly, experience fewer and similar numbers of coalescence events, and thus remain monodisperse. This physical insight agrees with the relative collision rate for NPs in solution. Specifically, the total collision rates are similar for both conventional and highly concentrated conditions (see Table S4) since the 5-fold higher diffusivity in the former is nearly offset by the 10-fold lower NP concentration. However, the relative collision rate (or the fraction of particles that collide, i.e., the ratio of the collision rate to the total number of particles) is nearly a factor of 6 higher for the conventional compared to the highly concentrated condition (see Table S4). The greater number of NPs undergoing coalescence events for the conventional condition supports the living coalescence process dominated by multiple coalescence events. In contrast, fewer NPs are involved in coalescence events for the high concentrations, promoting a step coalescence mechanism, more consistent reaction profiles per particle, and thus a more uniform size distribution.

CONCLUSION

We have shown that by concentrating precursor solutions near the solubility limit it becomes possible to separate precursor mixing and NP growth, and reproducibly achieve monodisperse NPs with a heat-up method. Within this new highly concentrated and viscous regime, synthesis parameters become less sensitive to experimental variability and thereby provide a reproducible and robust NP synthesis methodology. We demonstrated the intrinsic robustness of the method by showing that the NP synthesis is insensitive to chemical spikes (copper chloride and $Cu_{2-x}S$ seeds), which agree with an equivalent shift in the initial precursor ratios. Encouraged by the high degree of reproducibility and robustness of the highly concentrated reaction regime, we successfully scaled the reaction 2 orders of magnitude in volume to 2.5 L, all while maintaining an NP size and RSD similar to those observed on the laboratory scale. Importantly, the scale-up to a 215 g NP batch was accomplished with an unprecedented yield of 86 g of NPs/L of reaction volume. Furthermore, this method can be successfully adapted to other metal sulfides such as CdS and PbS. Our advances in the robust scale-up of colloidal NP synthesis derive from improved understanding of the interplay among chemical, thermal, and rheological properties on basic nucleation and growth. We point to the heat-up method under highly concentrated reaction environments as a promising NP synthesis methodology with significant potential to resolve outstanding challenges in producing NP materials at scales and capable of meeting their emerging demand.

ASSOCIATED CONTENT

Supporting Information

The Supporting Information is available free of charge on the ACS Publications website at DOI: 10.1021/jacs.5b10006.

Detailed experimental procedures, supporting characterization data, TEM images of the data, and physical and thermal property data (PDF)

AUTHOR INFORMATION

Corresponding Authors

*th358@cornell.edu
*rdr82@cornell.edu

Author Contributions

§C.B.W. and D.R.N. contributed equally to this work.

Notes

The authors declare no competing financial interest.

ACKNOWLEDGMENTS

This work was supported in part by the National Science Foundation (NSF) under Award No. CMMI-1344562. This work also made use of the Cornell Center for Materials Research Shared Facilities, which are supported through the NSF MRSEC (Materials Research Science and Engineering Centers) program (Grant DMR-1120296), and the KAUST-CU (KAUST-Cornell Center for Energy and Sustainability) prototyping laboratory, supported by the King Abdullah University of Science and Technology (KAUST) (Award No. KUS-C1-018-02).

REFERENCES

(1) Hendricks, M. P.; Campos, M. P.; Cleveland, G. T.; Jen-La Plante, I. J.; Owen, J. S. *Science* **2015**, *348*, 1226−1230.
(2) Park, J.; An, K.; Hwang, Y.; Park, J.-G.; Noh, H.-J.; Kim, J.-Y.; Park, J.-H.; Hwang, N.-M.; Hyeon, T. *Nat. Mater.* **2004**, *3*, 891−895.
(3) Kim, J. I.; Lee, J.-K. *Adv. Funct. Mater.* **2006**, *16*, 2077−2082.
(4) Cademartiri, L.; Bertolotti, J.; Sapienza, R.; Wiersma, D. S.; von Freymann, G.; Ozin, G. A. *J. Phys. Chem. B* **2006**, *110*, 671−673.
(5) Yuan, M.; Kemp, K. W.; Thon, S. M.; Kim, J. Y.; Chou, K. W.; Amassian, A.; Sargent, E. H. *Adv. Mater.* **2014**, *26*, 3513−3519.
(6) Du, Y.; Yin, Z.; Zhu, J.; Huang, X.; Wu, X.-J.; Zeng, Z.; Yan, Q.; Zhang, H. *Nat. Commun.* **2012**, *3*, 1177.
(7) Kang, X.; Yang, Y.; Huang, L.; Tao, Y.; Wang, L.; Pan, D. *Green Chem.* **2015**, *17*, 4482−4488.

DOI: 10.1021/jacs.5b10006
J. Am. Chem. Soc. 2015, 137, 15843−15851

(8) Protière, M.; Nerambourg, N.; Renard, O.; Reiss, P. *Nanoscale Res. Lett.* **2011**, *6*, 472.
(9) Flamee, S.; Cirillo, M.; Abe, S.; De Nolf, K.; Gomes, R.; Aubert, T.; Hens, Z. *Chem. Mater.* **2013**, *25*, 2476−2483.
(10) Zhang, J.; Gao, J.; Miller, E. M.; Luther, J. M.; Beard, M. C. *ACS Nano* **2014**, *8*, 614−622.
(11) Park, J.; Joo, J.; Kwon, S. G.; Jang, Y.; Hyeon, T. *Angew. Chem., Int. Ed.* **2007**, *46*, 4630−4660.
(12) Talapin, D. V.; Lee, J.-S.; Kovalenko, M. V.; Shevchenko, E. V. *Chem. Rev.* **2010**, *110*, 389−458.
(13) Kovalenko, M. V.; Manna, L.; Cabot, A.; Hens, Z.; Talapin, D. V.; Kagan, C. R.; Klimov, X. V. I; Rogach, A. L.; Reiss, P.; Milliron, D. J.; Guyot-sionnnest, P.; Konstantatos, G.; Parak, W. J.; Hyeon, T.; Korgel, B. a; Murray, C. B.; Heiss, W. *ACS Nano* **2015**, *9*, 1012−1057.
(14) Sun, L.; Choi, J. J.; Stachnik, D.; Bartnik, A. C.; Hyun, B.-R.; Malliaras, G. G.; Hanrath, T.; Wise, F. W. *Nat. Nanotechnol.* **2012**, *7*, 369−373.
(15) Owen, J. S.; Chan, E. M.; Liu, H.; Alivisatos, A. P. *J. Am. Chem. Soc.* **2010**, *132*, 18206−18213.
(16) Kwon, S. G.; Hyeon, T. *Small* **2011**, *7*, 2685−2702.
(17) Murray, C. B.; Norris, D. J.; Bawendi, M. G. *J. Am. Chem. Soc.* **1993**, *115*, 8706−8715.
(18) Murray, C. B.; Kagan, C. R.; Bawendi, M. G. *Annu. Rev. Mater. Sci.* **2000**, *30*, 545−610.
(19) Weidman, M. C.; Beck, M. E.; Hoffman, R. S.; Prins, F.; Tisdale, W. A. *ACS Nano* **2014**, *8*, 6363−6371.
(20) Zhang, H.; Hyun, B.-R.; Wise, F. W.; Robinson, R. D. *Nano Lett.* **2012**, *12*, 5856−5860.
(21) Perera, S. D.; Zhang, H.; Ding, X.; Nelson, A.; Robinson, R. D. *J. Mater. Chem. C* **2015**, *3*, 1044−1055.
(22) Kwon, S. G.; Piao, Y.; Park, J.; Angappane, S.; Jo, Y.; Hwang, N.-M.; Park, J.-G.; Hyeon, T. *J. Am. Chem. Soc.* **2007**, *129*, 12571−12584.
(23) van Embden, J.; Chesman, A. S. R.; Jasieniak, J. J. *Chem. Mater.* **2015**, *27*, 2246−2285.
(24) Joo, J.; Na, H. B.; Yu, T.; Yu, J. H.; Kim, Y. W.; Wu, F.; Zhang, J. Z.; Hyeon, T. *J. Am. Chem. Soc.* **2003**, *125*, 11100−11105.
(25) Zhang, H.-T.; Wu, G.; Chen, X.-H. *Langmuir* **2005**, *21*, 4281−4282.
(26) Jasieniak, J.; Bullen, C.; Van Embden, J.; Mulvaney, P. *J. Phys. Chem. B* **2005**, *109*, 20665−20668.
(27) Kruszynska, M.; Borchert, H.; Parisi, J.; Kolny-Olesiak, J. *J. Am. Chem. Soc.* **2010**, *132*, 15976−15986.
(28) Rempel, J. Y.; Bawendi, M. G.; Jensen, K. F. *J. Am. Chem. Soc.* **2009**, *131*, 4479−4489.
(29) Luther, J. M.; Jain, P. K.; Ewers, T.; Alivisatos, A. P. *Nat. Mater.* **2011**, *10*, 361−366.
(30) Lotfipour, M.; Machani, T.; Rossi, D. P.; Plass, K. E. *Chem. Mater.* **2011**, *23*, 3032−3038.
(31) Saldanha, P. L.; Brescia, R.; Prato, M.; Li, H.; Povia, M.; Manna, L.; Lesnyak, V. *Chem. Mater.* **2014**, *26*, 1442−1449.
(32) Leidinger, P.; Popescu, R.; Gerthsen, D.; Lünsdorf, H.; Feldmann, C. *Nanoscale* **2011**, *3*, 2544−2551.
(33) Russel, W. B.; Saville, D. A.; Schowalter, W. R. *Colloidal Dispersions*; Cambridge University Press: New York, 1989.
(34) Hanaor, D.; Michelazzi, M.; Leonelli, C.; Sorrell, C. C. *J. Eur. Ceram. Soc.* **2012**, *32*, 235−244.
(35) Xu, R.; Wu, C.; Xu, H. *Carbon* **2007**, *45*, 2806−2809.
(36) Ogawa, A.; Yamada, H.; Matsuda, S.; Okajima, K.; Doi, M. *J. Rheol. (Melville, NY, U. S.)* **1997**, *41*, 769.
(37) Srivastava, S.; Shin, J. H.; Archer, L. a. *Soft Matter* **2012**, *8* (15), 4097.
(38) Chieruzzi, M.; Cerritelli, G. F.; Miliozzi, A.; Kenny, J. M. *Nanoscale Res. Lett.* **2013**, *8*, 448.
(39) Xuan, Y.; Roetzel, W. *Int. J. Heat Mass Transfer* **2000**, *43*, 3701−3707.
(40) Xuan, Y.; Li, Q. *Int. J. Heat Fluid Flow* **2000**, *21*, 58−64.
(41) Talapin, D. V.; Rogach, A. L.; Haase, M.; Weller, H. *J. Phys. Chem. B* **2001**, *105*, 12278−12285.
(42) Finney, E. E.; Shields, S. P.; Buhro, W. E.; Finke, R. G. *Chem. Mater.* **2012**, *24*, 1718−1725.
(43) Wang, F.; Richards, V. N.; Shields, S. P.; Buhro, W. E. *Chem. Mater.* **2014**, *26*, 5−21.
(44) Lifshitz, I. M.; Slyozov, V. V. *J. Phys. Chem. Solids* **1961**, *19*, 35−50.
(45) Wagner, C. *Z. Elektrochem.* **1961**, *65*, 581−594.
(46) Huang, F.; Zhang, H.; Banfield, J. F. *J. Phys. Chem. B* **2003**, *107*, 10470−10475.
(47) Shields, S. P.; Richards, V. N.; Buhro, W. E. *Chem. Mater.* **2010**, *22*, 3212−3225.
(48) Burbelko, A. A.; Fraś, E.; Kapturkiewicz, W. *Mater. Sci. Eng., A* **2005**, *413*−*414*, 429−434.
(49) Avrami, M. *J. Chem. Phys.* **1941**, *9*, 177.
(50) Avrami, M. *J. Chem. Phys.* **1940**, *8*, 212.
(51) Avrami, M. *J. Chem. Phys.* **1939**, *7*, 1103.

DOI: 10.1021/jacs.5b10006
J. Am. Chem. Soc. 2015, 137, 15843−15851